Nanoscale

Self-Assembled Nitride-Metal Nanocomposites: Recent Progress and Future Prospects

Journal:	*Nanoscale*
Manuscript ID	NR-REV-09-2020-006316
Article Type:	Review Article
Date Submitted by the Author:	01-Sep-2020
Complete List of Authors:	Wang, Xuejing; Purdue University System, MSE Wang, Haiyan; Purdue University System, MSE; Neil Armstrong Engineering Building

Self-Assembled Nitride-Metal Nanocomposites: Recent Progress and Future Prospects

Xuejing Wang, Haiyan Wang

School of Materials Engineering, Purdue University, West Lafayette, IN 47907, USA

School of Electrical and Computer Engineering, Purdue University, West Lafayette, IN 47907, USA

Corresponding Author: hwang00@purdue.edu

Keywords: nitride-metal nanocomposite, self-assembly, plasmonic metamaterials, hybrid plasmonic materials

Abstract

Two-phase nanocomposites have gained significant research interests because of their multifunctionalities, tunable geometries and potential device applications. Different from the prior demonstrated oxide-oxide 2-phase nanocomposites, coupling nitride with metal presents high potentials of building alternative hybrid plasmonic metamaterials towards chemical sensing, tunable plasmonics, and nonlinear optics. Unique advantages, including distinct atomic interface, excellent crystalline quality, large-scale surface coverage and durable solid-state platform, address the high demands in new hybrid metamaterial designs for versatile optical material needs. This review summarizes the recent progress on nitride-metal nanocomposites, specifically targeting bottom-up self-assembled nanocomposite thin films. Various morphologies including vertically aligned nanocomposites (VAN), self-organized nanoinclusions, and nanoholes fabricated by additional chemical treatment are introduced. Starting from thin film nucleation and growth, the prerequisites of successful strain coupling and the underlying growth mechanisms are discussed. These findings facilitate a better control of tunable nanostructures and optical functionalities. Future research directions are proposed, including morphological control of secondary phase to enhance its homogeneity, coupling nitride with magnetic phase for magneto-optical effect as well as growing all-ceramic nanocomposites to extend the functionalities and anisotropy.

Introduction

Nanocomposite thin films present a coupled thin film platform between two or more material components at nanoscale, in many cases, realized by bottom-up vapor deposition techniques.[1-3] Various nanocomposite thin film morphologies have been demonstrated including nanoparticles, multilayers and vertically aligned nanocomposites (VAN).[4-7] In particular, VANs have drawn great attentions recently because of their unique vertical nanostructures, versatile coupled functionalities, strong vertical strain couplings, and tunable anisotropic physical properties.[8-11] Some of the major advantages of the two-phase nanocomposites include the geometrical tunability and flexible materials selections. Growth parameters such as laser energy and frequency, background pressure, substrate temperature and post-deposition annealing have been demonstrated for tailored morphologies and 2-phase distributions.[9, 12-16]

In term of materials selections, much of the VAN work has been focusing on oxide-oxide demonstrations including $BaTiO_3$ (BTO)-based,[17-18] $BiFeO_3$ (BFO)-based,[19-20] $La_{0.7}Sr_{0.3}MnO_3$ (LSMO)-based[21-23] VAN systems. Recently, a new class of oxide-metal VAN has been demonstrated for enhanced anisotropic physical properties by coupling a functional metallic phase in the VAN structure. Specifically, plasmonic metal (e.g., Au, Ag, Cu) with very strong surface plasmon modes have been incorporated with oxides in VANs such as enhanced plasmonic resonance in BTO-Au, ZnO-Ag_xAu_{1-x}, ZnO-Cu, their superior optical anisotropy, tunable geometries and compatibility for Si integration could be very useful towards novel nanophotonic applications.[24-31] Magnetic metal (e.g., Co, Ni, Fe) with strong spin polarization effect have been successfully integrated in oxides as well, such as magnetic anisotropy in $BaZrO_3$ (BZO)-Co, tunable ionic conductivities in CeO_2-Ni and enhanced magnetoresistance properties in BTO-Fe by coupling with functional layers such as $YBa_2Cu_3O_{7-x}$ or LSMO have

been demonstrated.[32-35] These novel nanostructures could be of great interest towards memristors, spintronics, and ultrafast switching devices.[36-39]

Considering the urgent needs of high temperature plasmonic and photonic nanostructures, another new class of VAN systems using nitrides as one of the nanocomposite phases has been demonstrated recently, including TiN-Au, TaN-Au, TiN-Ag, AlN-Au, AlN-Ag, TiN-AlN, etc.[40-44] As an example, TiN is conventionally being used for superhard coating and diffusion barrier,[45-48] and is CMOS compatible for gate electrodes.[49] Recent studies suggest that TiN nanostructures exhibit comparable plasmonic properties to Au while much higher endurance to irradiation or thermal treatments.[50-52] Thus, nitride-based VANs have evolved as a new class of thermally stable, plasmonic and hyperbolic metamaterials.

Part I: Prerequisites for nitride-metal nanocomposite growth

Figure 1 plots the real part dielectric constant (ε_1) at the optical wavelength of 500 nm versus the lattice parameter of the common nitride and metal candidates. The vertical dashed lines are lattice parameters of three substrate crystals including STO, MgO and *c*-cut sapphire. As a model system, TiN could serve as an ideal candidate for plasmonic-based device applications under extreme conditions as well as a durable ceramic matrix that supports the growth of secondary phase. Different nanostructures composed of single-phase noble metals (i.e., Au, Ag) and TiN are shown in Figure 1 panel (A), where distinct features down to 100 nm can be patterned by lithographic method.[53-58] Two-phase heterostructures such as metal-metal hybrids (Au-Ag)[59], nitride-nitride multilayer (TiN-AlN)[6, 43] as well as nitride-oxide hybrid (TiN-VO_2)[60] provide fruitful ideas and experiences for growing nitride-metal VAN thin films. As a comparison, the self-assembled thin films of nitride-metal VANs (Figure 1 C) compensate the lossy and unstable metal phase and bring engineerable plasmonic properties. Similar to the oxide-oxide

nanocomposite thin film growth,[1-2] the prerequisites of two constituent phases for achieving successful nitride-metal VANs include: (1) comparable crystal symmetry and lattice parameters at film interface and the film/substrate interface; (2) different nucleation energy or wetting properties, i.e., islanded growth for nanopillars and layered growth for matrix; (3) no chemical reaction or interdiffusion; (4) matrix phase participates at least 50% volume ratio of the composite target.

The nitride family can be categorized by the charge carrier density, i.e., semiconducting III-V nitrides such as AlN and GaN, metallic transition-metal-nitrides such as TiN and ZrN. Based on that, two nitride-metal nanocomposite configurations have been presented: (1) coupling transition-metal-nitride (e.g. TiN) with metal towards tunable plasmonics, enhanced durability and sensing applications; (2) coupling III-V nitride with metal towards extreme optical anisotropy or bandgap tuning. An overview of nitride-metal in Figure 1(C) with examples on tailoring density and tilting angles of the 2nd phase, nanohole processing are presented. In the following sections, we will review the recently reported nitride-based VAN systems and their unique morphologies (Part II). Different structures are demonstrated depending on the different nitride matrices selected. Tunabilities in terms of pillar density, distribution and angular tilting are summarized in Part III, and correlated with their novel optical properties (Part IV). Last, a recent demonstration of nanohole framework is presented based on further processing of the nitride-metal systems (Part V). Summary and future research perspectives will be discussed in Part VI.

Part II: Three-dimensional strain, nucleation and growth

2.1 Transition metal nitride - metal nanocomposites

The initial success of growing nitride-metal nanocomposites started with TaN-Au and TiN-Au systems using the co-growth method of pulsed laser deposition.[42] From plan-view and cross-section images (Figure 2a-d), Au nanopillars are distinctly and uniformly distributed vertically inside the nitride matrix, with an average diameter of 5 nm and inter-pillar distance of 10 nm. High crystallinity is revealed by cube-on-cube stacking of atomic plane along *c*-axis without in-plane rotation or sub-diffraction peaks. Several factors including strain, nucleation energy and inherit material properties are intercorrelated and attributed to the formation of such self-assembled nitride-metal VAN. Specifically, the lattice parameters of TaN (a_{TaN} = 4.37 Å), TiN (a_{TiN} = 4.24 Å), Au (a_{Au} = 4.07 Å) and MgO substrate (a_{MgO} = 4.21 Å) provide a close matching condition from three dimensions, i.e., at the nitride/metal boundary along vertical interface and at the film/substrate interface along horizontal interface (Figure 2e). As a comparison, Au nanopillars in TaN exhibit a more pronounced hexagonal in-plane ordering. In terms of surface energy, metals favor island growth mode while nitrides tend to follow the 2D layered growth mode. In most occasions, the self-assembly mechanism involves two steps (Figure 2f), formation of the seed layer as preferable mode and continuous growth of the VAN film. The differences in nucleation surface energy thus become crucial factors determining the pillar-in-matrix formation. One additional benefit of nitride-metal VAN is that compare to most oxides, transition-metal-nitrides are rather stable against thermal, mechanical or irradiation treatments.

2.2 III-V nitride – metal nanocomposites

The difference in crystal symmetry and lattice constant results in a change of growth scenario when coupling III-V nitride with metals.[44] For example, pure AlN (wurtzite) nucleates on top of *c*-cut sapphire (hexagonal) substrate shows an out-of-plane interfacial strain of ~14.25%, with 30 ° rotated matching along *c*-axis (2i).[61-62] This posts challenges in integrating another cubic metal

phase such that the crystallinity and geometrical homogeneity could be affected by the strain. As a result, morphologies of AlN-metal (Au, Ag) two-phase nanocomposites appear as self-organized metal nanoinclusions being embedded in nitride matrix, according to the STEM micrographs shown in Figure 2(g,h), but the overall crystallinity is maintained as highly textured.[44] Specifically, two-step growth stages have been involved. The initial 15 nm growth is highly strained where Au and Ag nucleate as ultrafine and ordered particles to partially release the strain energy at the AlN/sapphire interface. At the second stage, the interfacial strain is relaxed, which leads to the agglomeration of metal nanoinclusions depending on the surface energies and strain of the metal phase. As illustrated in Figure 2(i), both Au or Ag prefer the (111) nucleation considering their lowest surface energy as well as lattice matching with AlN.[63]

2.3 Strain and surface energy affected growth morphology

The three-dimensional strain evolved during the nanocomposite growth is critical in controlling the morphology and defects states, thus, identifying the interfacial strain at atomic scale helps to understand the underlying mechanism of the growth. As described earlier, the unique hexagonal pattern in TaN-Au is resulted from a strain compensation model, a balance between ~3.68% compressive strain at TaN/MgO interface and ~3.55% tensile strain at Au/MgO interface facilitate a well-spaced nucleation of Au nanopillars in the TaN matrix. It is proposed that the nucleation of Au follows the misfit dislocation cores at TaN/MgO interface. In general, both TaN-Au and TiN-Au grown on MgO substrates exhibit desirable matching conditions, and have been observed at in-plane (Figure 3a,c) and out-of-plane (b) directions. The perfect lattice matching helps minimize the surface and strain energies, providing stable templates for further processing such as chemical etching in producing TiN nanoholes.[64] The interface at TiN/Ag nanocomposite, on the other hand, is rather faceted and shifted along with the atomic plane

stacking (Figure 3d). Such morphology is resulted from a competition between thermal and kinetic energy. The tilting is facilitated by reduced growth rate which enables more aggressive adatom diffusion laterally and/or the exposure of low-energy surfaces. In most cases, the high kinetic energy of the pulsed laser dominates the growth and force the nanopillars to be aligned vertically.

Part III: Tailorable nanostructures and properties in nitride-metal VANs

3.1 Density tuning of metallic nanopillars in nitride-metal VANs

TiN and Au are dissimilar materials and exhibit distinct optical properties at ultraviolet to near-infrared (UV-NIR) region. Thus, tuning the density of Au within TiN-Au platform becomes an intuitive way to control the charge carrier density and the dielectric function in the nanocomposites. In addition, the VAN structure could create strong anisotropy compare to pure TiN and Au thin films. Realizing density tuning of Au can be achieved by changing the volume ratio of Au within the composite target. The microstructures of as-grown TiN-Au VAN films with three different densities are displayed in Figure 4, where low density results in thinner and sparsely distributed Au nanopillars while high density results in broader and densely packed ones, the overall volume fraction is increased gradually from Figure 4(a-c).[40] The hybrid thin film surfaces can be considered as artificially built metasurfaces and the change of morphology affected by Au density bring tunable sensing capabilities. From cross-sectional images (Figure 4 d-f), the nanopillars are vertically aligned with distinct interface, a cube-on-cube epitaxy is confirmed as shown in the selected area electron diffraction (SAED) patterns. Such high-quality growth of VAN is resulted from a near perfect lattice match at TiN/MgO interface (<1%).

Explorations on fundamental optical properties presented in Figure 5 suggest tunable plasmonic resonance, charge carrier concentration, as well as anisotropic dielectric function. Surface plasmon resonance (SPR) of pure TiN and pure Au film are located at 375 nm and 500 nm (Figure 5a), respectively. By increasing the density of Au within TiN matrix, a gradual red shift of the transmittance peak is revealed. Geometrical control in tuning the plasmonic resonance frequency has been extensively explored in chemically synthesized nanoparticles to improve the detection limit of the biosensors.[65-67] Here, the real part dielectric function (Figure 5b) of TiN-Au VANs retrieved from a single-layer model reveals a gradual shift of plasma frequency (ω_p) with change of Au density, which is correlated with the tuning of charge carrier concentration. In general, TiN-Au VANs are less metallic compare to pure TiN or Au film, strain energy or scattering at TiN/Au interface could be the contributed factors. Interestingly, the fitted dielectric function into uniaxial tensors (Figure 5c,d) exhibit strong variations between ordinary (ε_1^o) and extraordinary terms (ε_1^{eo}), such anisotropy within nanocomposite composed of pure plasmonic phases is owing to the unique pillar-in-matrix geometry and difference in carrier concentration of TiN and Au. The oscillations along *c*-axis (ε_1^{eo}) can be correlated to the vertical strain coupling at TiN/Au. Achieving anisotropy and tunability within plasmonic platform is very interesting considering the impact of dielectric function or electromagnetic field distribution along vertical boundaries, building physical models using method such as *ab initio* would be important in understanding the atomic coupling at the nitride/metal interface.[68]

3.2 Morphology tuning from three-dimensions in nitride-metal VANs

Compare to the density tuning, achieving tilted nanopillar array within TiN matrix is much more challenging. Previous reports on tilted nanorod-like plasmonic nanostructures are limited to single-phase, techniques such as slanting angle deposition or nanolithography patterning but

exhibit certain limitations in terms of morphology control or output scale.[53, 69-71] The specific TiN-Ag VAN realizes such tilted nanopillar design due to the inherit thermodynamics of Ag as well as a careful control of growth parameters.[41] Figure 6 display three-dimensional microstructures of TiN-Ag nanocomposites with Ag nanopillars tilted at 0° (Figure 6a,d), 25° (b,e) and 50° (c,f). From the plan-view, a transition from rounded dots to elongated rods with increase of tilting angle is revealed, which is more obvious from the cross-sectional projections. Distinct pillar arrays are grown without interdiffusion or intermixing which indicates effective two-phase coupling between TiN and Ag. The SAED patterns further confirm the high crystalline nature of the hybrid films. The underlying mechanism is attributed to both thermodynamics and kinetics. While high kinetic energy of laser could dominate the vertical alignment of the ultrathin pillars, reducing the growth rate by increasing growth temperature and/or enlarging the substrate-target distance support longer resting time for adatom diffusion, thus allowing lateral shifting of adatoms to reduce the surface energy towards more thermally favorable growth state. The complementary effect includes the pillar diameter as well as the overall film thickness.

Strong surface enhanced Raman scattering (SERS) and surface plasmon (SP) modes make Ag a more favorable than other metals for plasmonic sensing.[72] Taking advantage of the three-dimensional anisotropic structure, TiN-Ag hybrid thin film platform has been demonstrated with angular selective reflectivity covering the entire UV-IR range.[41] The real measurements were conducted by collecting angular dependent reflectance spectra with sample rotated at 180°, namely, with light propagating facing (30° to 70°) or along (-30° to -70°) the tilted pillar interface as illustrated in Figure 7. At visible frequencies (Figure 7 a,b), such anisotropy is observed by the changes of the overall intensity as well as the sharpness of the resonance dip at

400 nm. The 2D electric field maps (insets of Figure 7a,b) retrieved at 420 nm indicate that a stronger SP resonance when light shining onto the tilted Ag, and reduced field intensity along the opposite direction that is caused by extinction or scattering at the TiN/Ag interface. The overall maximum reflectance is achieved at -30° incidence, which is also confirmed by the similar measurements conducted at infrared regime. Three selected wavelengths at 3 μm, 5 μm and 8 μm demonstrate the consistency of such angular selective response as indicated by the red arrows shown in Figure 7(c). Angular selectivity is crucial towards plasmonic nanoantenna designs, the tilted TiN-Ag nanocomposites have proved to be a promising candidate.[73-74] Towards more effective sensing, the inhomogeneity such as uniformity of the tilting direction as well as interpillar distances can be improved, more investigations on growth parameter control and/or template assisted ordering by additional treatment are interesting to explore.[75-76]

Part IV. Versatile functionalities demonstrated in Nitride-Metal VANs

The nitride-metal VANs are multifunctional and can be further incorporated with other nanostructures towards complex designable metamaterials and devices. Preliminary explorations have demonstrated multifunctionalities including thermal and mechanical durability, surface plasmon enhanced sensing, as well as nonlinearity. These demonstrations could open a plethora of design opportunities since the development of nitride-metal nanocomposites is still in their early stage. New physics phenomena (e.g. quantum plasmonics) and functionalities potentially involved should be further understood upon future experimental explorations and modeling.[77-79]

4.1 Mechanical and thermal stability

Metals such as Ag, Al or Cu are mechanically soft and could be easily degraded or reacted upon mechanical or thermal fluctuations. Such instability issues could be resolved partially by

designing hybrid nanostructures such as core-shell nanoparticles. Protecting unstable core using more stable candidates like Au, graphene have been reported to enhance the overall stability and signal-to-noise ratios of SERS detection.[59, 67, 80-81] Similarly, VANs could be ideal in terms of embedding the metallic nanowire or nanopillar array within a mechanically strong matrix. Compared to the reported oxide-metal designs, applying robust nitrides as the host matrix is more effective in preventing interdiffusion or chemical reaction. As demonstrated in the TiN-Ag VAN system,[41] both elastic modulus and hardness values (Figure 8a-b) are comparable to those of pure TiN film, which is a surprising enhancement considering the soft Ag and the rule-of-mixture hardness of TiN-Ag nanocomposites. In the presented study, thermal stability was tested both *ex-situ* and *in-situ*, results shown in Figure 8(c) present the *in-situ* emittance spectra measured at three temperatures, and the microstructure (inset) after heating exhibits high crystallinity without obvious morphological change.

4.2 Surface plasmon enhanced sensing

The nitride-metal VANs provide a unique morphology that the metal nanopillars protruded onto the surface could be highly functional for chemical detection or biomedical sensing, taking advantage of the SERS effect. To this end, Raman scattering (Figure 8d,e) measured in TaN-Au and TiN-Au VANs demonstrate significant enhancement of the signal over the entire measurement range compare to the pure TaN and TiN thin films.[42] The strong localized surface plasmon resonance (LSPR) modes of the protruded Au nanopillars act as active resonance center to enhance the electric field. These active nanoresonators can be utilized for effective detection of the chemical bonds. As demonstrated by Wang *et al.*,[40] chemical treatment at the thin film surface enables attachment between Au and the target analytes. In this case, the -OH stretching from methanol located at near 3000 cm^{-1} is effectively detected. Furthermore (data not shown), a

set of surface cover-recover process using 3-mereaptopropionic acid (MPA) functionalization was conducted to demonstrate that such detection comes primarily from Au instead of TiN, which shows a density dependency. Comparison between these TiN-Au to colloidal liquid-based nanoparticles suggest the high sensitivity of TiN-Au VANs possibly contributed by the uniformly distributed nanopillars. Additionally, these solid-state templates are reusable and more robust against chemical treatments compare to liquid-based samples.

4.3 Nonlinearity demonstrated in nitride-metal VANs

Nonlinear plasmonics generally describe the anharmonicity of electromagnetic field, 2nd and 3rd order nonlinearities are of special importance towards ultrafast switching and wave manipulations.[82] Second and third harmonic generation (SHG) has been reported in TiN nanoantennas.[58, 83] For continuous nitride films, only weak nonlinearity has been detected that is correlated to the strain induced lattice distortions. Nitride-metal nanocomposites generates non-centro-symmetry within the structure such that the SHG signals of output polarization at 0° and 90° in TaN-Au show dramatic enhancement compare to the pure TaN film (Figure 8 g,h). Similar response has been observed in the 50° tilted TiN-Ag nanocomposites (Figure 8i). Factors could be related to the alignment of the nanopillars as well as the strained coupling at the pillar/matrix interface. Such nonlinearity property observed in nitride-metal VANs with both centro-symmetry phases, suggests the inversion symmetry breaking based on the vertical strain coupling and lattice distortion in the VANs. Further understanding the mechanisms through modeling efforts could be of great interests.

Part V. Beyond nitride-metal nanocomposites

5.1 Large-scale fabrication of nitride-based nanoholes

Taking advantage of the high-quality TiN-Au VANs and high chemical inertness of TiN, additional processing using chemical etching can selectively etch away Au nanopillars and leave the robust TiN as a large-scale nanohole template.[64] A similar treatment in producing porous oxide template has been demonstrated in a oxide-oxide VAN by water dissolution of one phase.[84] Compare to the previous demonstrations using lithographic patterning, colloidal or alumina template assisted coating and nanoimprinting method,[85-88] this unique nanohole fabrication method presents multiple advantages including large-scale throughput, sub-10 nm feature size, superior hardness and chemical inertness. It is also interesting to note that the etching process can be stopped half way or fully etched as shown in Figure 9(a-f).[64] Sharp features with diameter of 6 nm are visualized, and the nanoholes maintain the distinct morphology without being damaged upon strong acid etching. As introduced, the removal of Au induces a strong in-plane relaxation thus the selection of MgO substrate is crucial to minimize the interfacial strain and avoid stress induced lattice distortion upon chemical etching.

Plasmonic nanoholes generate extraordinary optical transmission (EOT) and surface plasmon (SP) modes that can be applied for microfluid sensors.[89-93] Specifically, the strong SP modes compare TiN nanohole with TiN-Au VAN show significant enhancement of electric field localization (Figure 9g). As the Au nanopillars being replaced by “air holes”, a strong optical anisotropy is generated which becomes more pronounced at higher wavelengths (> 1500 nm). Interestingly, these nanoholes are capable to absorb small droplets (nanocapillary effect) of liquid and the edges of nanohole interface is extremely sensitive to the local change of refractive index (Figure 9i), with resulted specular shift per refractive index unit (RIU) of 127.43 and 258.86 nm, respectively. Moreover, TiN nanoholes as periodic nanocavities or defect sites would affect the crystallization process of the 2D perovskite nanoplates nucleated on top. Enhanced

photoluminescence (PL) signal and new peaks are generated as a result of defective surface topology offered by the nanohole plasmonic metasurface (Figure 9j). The underlying mechanism is rather sophisticated, but the presented work demonstrates the novelty of the fabrication towards potential applications of plasmonic sensing.

Part VI: Summary and future perspectives

6.1 Summary

Based on above review, nitride-based VAN systems have presented as a new VAN family coupling the unique structural and physical properties of nitrides with plasmonic metals. Besides the novel optical properties presented by the nitride-based VANs, the growth and morphology of nitride-metal nanocomposites also allow a better understanding on growth mechanisms and interfacial coupling at atomic resolution for VANs. Such understanding helps realizing tailorable geometries and bring new design possibilities using this bottom-up thin film growth approach. The advantages including good epitaxial quality, large-scale throughput and sub-10 nm feature size are not easily obtained in existing fabrication methods such as lithographic patterning or porous templated growth. Realizing controllable nanostructures is very attractive towards tunable plasmonics and metamaterial designs, preliminary demonstrations on optical anisotropy, tunable carrier density, chemical bonding detection, thermal and mechanical durability all present high potential for plasmonic metamaterial-based applications such as sensing, nonlinear optics, high-temperature plasmonics, and nanophotonic chips. Future studies in the areas of improving the periodicity or homogeneity of the nitride-metal nanocomposites, coupling nitrides with alloyed or magnetic metals, and all-ceramic nanocomposites could be valuable to explore as outlined below.

6.2 Precise morphology control

As most of the nanocomposites are grown via a self-assembly process, one of the main challenges for VAN growth is achieving periodicity or ordering between the two constituent phases. Effective manipulation over wavefront (e.g. polarization and refraction) requires specific design parameters, i.e., the distance and shape of nanoresonators.[94-95] Thus, minimizing inhomogeneity, such as packing distance, dimension, or the tilting angles, could have major impacts on the resonance wavelength, detection sensitivity, and angular selectivity. Improving the periodicity requires more careful control over strain and crystal symmetry of the material candidates or using additional treatments to facilitate the ordering. Specifically, either using lithography to pattern periodic "defect" sites for directed nucleation, or using templated substrates has been demonstrated as an effective way to achieve ordered oxide-oxide VAN growth.[75-76] These methods can be implemented for nitride-metal growth to achieve ordered growth.

6.3 Incorporating magnetic metals and alloys

Towards magnetic data storage, ultrafast switching and spintronic devices, magnetic metals, bottom-up growths coupling Co, Ni nanopillars with BZO or CeO_2 have already been demonstrated, showing the strong magnetic anisotropy and enhanced ferromagnetism affected by the vertically alignment of the magnetic nanopillars. Magnetic nanowires grown in porous alumina template have demonstrated the unique magneto-optical (MO) coupling and Kerr effect.[39, 96] Compare to oxide templates, TiN is paramagnetic and serves as a durable matrix since metals like Co or Ni are not as stable as Au when grown under high temperature. Plasmonic enhancement of magnetic spin polarization could be possible as TiN is supporting strong SP mode.

6.4 Metal-free ceramic-ceramic nanocomposites

Aside from the instability issue, metamaterials involving metallic components are always lossy at optical frequencies.[97] Compensating the losses using gain media or engineering the geometry of design and developing better plasmonic candidates to replace metals have been proposed as effective solutions.[52, 98] It could be possible to use all-ceramic candidates with dissimilar properties such as the carrier density and mobility.[99] TiN or doped oxides (e.g. ITO, ZnO) have been demonstrated as promising alternative plasmonic candidates,[100-101] incorporating those with another ceramic phase as VANs could be challenging but can possibly be realized via careful growth control. Very recently a new ceramic-ceramic hyperbolic metamaterial of NiO-TiN VANs has been demonstrated. NiO is semiconducting and weak ferromagnetic phase filling as tunable nanorods array, and enables hyperbolic transitions and plasmonic enhanced spin polarization (MO) effect.[102] The new nitride-based ceramic-ceramic hybrid material designs could open up enormous opportunities in new plasmonic and optical material designs, and thus worth further exploration.

Acknowledgement

This work was supported by the U.S. National Science Foundation (DMR-2016453 for thin film processing and DMR-1565822 for the high resolution TEM and STEM effort). This work was partially supported by the Basil R. Turner Professorship at Purdue University.

References

(1) MacManus-Driscoll, J. L., Self-Assembled Heteroepitaxial Oxide Nanocomposite Thin Film Structures: Designing Interface-Induced Functionality in Electronic Materials. *Advanced Functional Materials* **2010,** *20* (13), 2035-2045.
(2) Zhang, W.; Chen, A.; Bi, Z.; Jia, Q.; MacManus-Driscoll, J. L.; Wang, H., Interfacial coupling in heteroepitaxial vertically aligned nanocomposite thin films: From lateral to vertical control. *Current Opinion in Solid State and Materials Science* **2014,** *18* (1), 6-18.
(3) Huang, J.; MacManus-Driscoll, J. L.; Wang, H., New epitaxy paradigm in epitaxial self-assembled oxide vertically aligned nanocomposite thin films. *Journal of Materials Research* **2017,** *32* (21), 4054-4066.
(4) Jian, J.; Wang, X.; Misra, S.; Sun, X.; Qi, Z.; Gao, X.; Sun, J.; Donohue, A.; Lin, D. G.; Pol, V.; Youngblood, J.; Wang, H.; Li, L.; Huang, J.; Wang, H., Broad Range Tuning of Phase Transition Property in VO2 Through Metal-Ceramic Nanocomposite Design. *Advanced Functional Materials* **2019,** *29* (36), 1903690.
(5) Lu, D.; Kan, J. J.; Fullerton, E. E.; Liu, Z., Enhancing spontaneous emission rates of molecules using nanopatterned multilayer hyperbolic metamaterials. *Nature Nanotechnology* **2014,** *9* (1), 48-53.
(6) Naik, G. V.; Saha, B.; Liu, J.; Saber, S. M.; Stach, E. A.; Irudayaraj, J. M. K.; Sands, T. D.; Shalaev, V. M.; Boltasseva, A., Epitaxial superlattices with titanium nitride as a plasmonic component for optical hyperbolic metamaterials. *Proceedings of the National Academy of Sciences* **2014,** *111* (21), 7546-7551.
(7) Macmanus-Driscoll, J. L.; Foltyn, S. R.; Jia, Q. X.; Wang, H.; Serquis, A.; Civale, L.; Maiorov, B.; Hawley, M. E.; Maley, M. P.; Peterson, D. E., Strongly enhanced current densities in superconducting coated conductors of YBa2Cu3O7–x + BaZrO3. *Nature Materials* **2004,** *3* (7), 439-443.
(8) Zhang, W.; Ramesh, R.; MacManus-Driscoll, J. L.; Wang, H., Multifunctional, self-assembled oxide nanocomposite thin films and devices. *MRS Bulletin* **2015,** *40* (9), 736-745.
(9) Chen, A.; Bi, Z.; Tsai, C.-F.; Lee, J.; Su, Q.; Zhang, X.; Jia, Q.; MacManus-Driscoll, J. L.; Wang, H., Tunable Low-Field Magnetoresistance in (La0.7Sr0.3MnO3)0.5:(ZnO)0.5 Self-Assembled Vertically Aligned Nanocomposite Thin Films. *Advanced Functional Materials* **2011,** *21* (13), 2423-2429.
(10) Chen, A.; Bi, Z.; Jia, Q.; MacManus-Driscoll, J. L.; Wang, H., Microstructure, vertical strain control and tunable functionalities in self-assembled, vertically aligned nanocomposite thin films. *Acta Materialia* **2013,** *61* (8), 2783-2792.
(11) Chen, A.; Su, Q.; Han, H.; Enriquez, E.; Jia, Q., Metal Oxide Nanocomposites: A Perspective from Strain, Defect, and Interface. *Advanced Materials* **2019,** *31* (4), 1803241.
(12) Chen, A. P.; Zhang, W. R.; Khatkatay, F.; Su, Q.; Tsai, C. F.; Chen, L.; Jia, Q. X.; MacManus-Driscoll, J. L.; Wang, H., Magnetotransport properties of quasi-one-dimensionally channeled vertically aligned heteroepitaxial nanomazes. *Appl. Phys. Lett.* **2013,** *102* (9), 4.
(13) Macmanus-Driscoll, J. L.; Zerrer, P.; Wang, H.; Yang, H.; Yoon, J.; Fouchet, A.; Yu, R.; Blamire, M. G.; Jia, Q., Strain control and spontaneous phase ordering in vertical nanocomposite heteroepitaxial thin films. *Nature Materials* **2008,** *7* (4), 314-320.
(14) Paldi, R. L.; Sun, X.; Wang, X.; Zhang, X.; Wang, H., Strain-Driven In-plane Ordering in Vertically Aligned ZnO–Au Nanocomposites with Highly Correlated Metamaterial Properties. *ACS Omega* **2020,** *5* (5), 2234-2241.

(15) Zhang, D.; Misra, S.; Li, L.; Wang, X.; Jian, J.; Lu, P.; Gao, X.; Sun, X.; Qi, Z.; Kalaswad, M.; Zhang, X.; Wang, H., Tunable Optical Properties in Self-Assembled Oxide-Metal Hybrid Thin Films via Au-Phase Geometry Control: From Nanopillars to Nanodisks. *Advanced Optical Materials* **2020,** *8* (4), 1901359.
(16) Mohaddes-Ardabili, L.; Zheng, H.; Ogale, S. B.; Hannoyer, B.; Tian, W.; Wang, J.; Lofland, S. E.; Shinde, S. R.; Zhao, T.; Jia, Y.; Salamanca-Riba, L.; Schlom, D. G.; Wuttig, M.; Ramesh, R., Self-assembled single-crystal ferromagnetic iron nanowires formed by decomposition. *Nature Materials* **2004,** *3* (8), 533-538.
(17) Khatkhatay, F.; Chen, A.; Lee, J. H.; Zhang, W.; Abdel-Raziq, H.; Wang, H., Ferroelectric Properties of Vertically Aligned Nanostructured BaTiO3–CeO2Thin Films and Their Integration on Silicon. *ACS Applied Materials & Interfaces* **2013,** *5* (23), 12541-12547.
(18) Gao, X.; Zhang, D.; Wang, X.; Jian, J.; He, Z.; Dou, H.; Wang, H., Vertically aligned nanocomposite (BaTiO3)0.8 : (La0.7Sr0.3MnO3)0.2 thin films with anisotropic multifunctionalities. *Nanoscale Advances* **2020,** *2* (8), 3276-3283.
(19) Aimon, N. M.; Hun Kim, D.; Kyoon Choi, H.; Ross, C. A., Deposition of epitaxial BiFeO3/CoFe2O4 nanocomposites on (001) SrTiO3 by combinatorial pulsed laser deposition. **2012,** *100* (9), 092901.
(20) Stratulat, S. M.; Lu, X.; Morelli, A.; Hesse, D.; Erfurth, W.; Alexe, M., Nucleation-Induced Self-Assembly of Multiferroic BiFeO 3 –CoFe 2 O 4 Nanocomposites. **2013,** *13* (8), 3884-3889.
(21) Sun, X.; Huang, J.; Jian, J.; Fan, M.; Wang, H.; Li, Q.; Mac Manus-Driscoll, J. L.; Lu, P.; Zhang, X.; Wang, H., Three-dimensional strain engineering in epitaxial vertically aligned nanocomposite thin films with tunable magnetotransport properties. *Materials Horizons* **2018,** *5* (3), 536-544.
(22) Zhang, W.; Chen, A.; Khatkhatay, F.; Tsai, C.-F.; Su, Q.; Jiao, L.; Zhang, X.; Wang, H., Integration of Self-Assembled Vertically Aligned Nanocomposite (La0.7Sr0.3MnO3)1–x:(ZnO)x Thin Films on Silicon Substrates. *ACS Applied Materials & Interfaces* **2013,** *5* (10), 3995-3999.
(23) Zhang, W.; Li, L.; Lu, P.; Fan, M.; Su, Q.; Khatkhatay, F.; Chen, A.; Jia, Q.; Zhang, X.; Macmanus-Driscoll, J. L.; Wang, H., Perpendicular Exchange-Biased Magnetotransport at the Vertical Heterointerfaces in La 0.7 Sr 0.3 MnO 3 :NiO Nanocomposites. **2015,** *7* (39), 21646-21651.
(24) Li, L.; Sun, L.; Gomez-Diaz, J. S.; Hogan, N. L.; Lu, P.; Khatkhatay, F.; Zhang, W.; Jian, J.; Huang, J.; Su, Q.; Fan, M.; Jacob, C.; Li, J.; Zhang, X.; Jia, Q.; Sheldon, M.; Alu, A.; Li, X.; Wang, H., Self-Assembled Epitaxial Au-Oxide Vertically Aligned Nanocomposites for Nanoscale Metamaterials. *Nano Lett* **2016,** *16* (6), 3936-43.
(25) Misra, S.; Li, L.; Zhang, D.; Jian, J.; Qi, Z.; Fan, M.; Chen, H.-T.; Zhang, X.; Wang, H., Self-Assembled Ordered Three-Phase Au–BaTiO3–ZnO Vertically Aligned Nanocomposites Achieved by a Templating Method. *Advanced Materials* **2019,** *31* (7), 1806529.
(26) Paldi, R. L.; Wang, X.; Sun, X.; He, Z.; Qi, Z.; Zhang, X.; Wang, H., Vertically Aligned AgxAu1–x Alloyed Nanopillars Embedded in ZnO as Nanoengineered Low-Loss Hybrid Plasmonic Metamaterials. *Nano Lett.* **2020,** *20* (5), 3778-3785.
(27) Huang, J.; Wang, X.; Phuah, X. L.; Lu, P.; Qi, Z.; Wang, H., Plasmonic Cu nanostructures in ZnO as hyperbolic metamaterial thin films. *Materials Today Nano* **2019,** *8*, 100052.
(28) Kalaswad, M.; Zhang, D.; Gao, X.; Contreras, L. L.; Wang, H.; Wang, X.; Wang, H., Integration of Hybrid Plasmonic Au–BaTiO3 Metamaterial on Silicon Substrates. *ACS Applied Materials & Interfaces* **2019,** *11* (48), 45199-45206.

(29) Nicholls, L. H.; Rodríguez-Fortuño, F. J.; Nasir, M. E.; Córdova-Castro, R. M.; Olivier, N.; Wurtz, G. A.; Zayats, A. V., Ultrafast synthesis and switching of light polarization in nonlinear anisotropic metamaterials. *Nat. Photonics* **2017,** *11* (10), 628-633.
(30) Yao, J.; Liu, Z.; Liu, Y.; Wang, Y.; Sun, C.; Bartal, G.; Stacy, A. M.; Zhang, X., Optical Negative Refraction in Bulk Metamaterials of Nanowires. *Science* **2008,** *321* (5891), 930-930.
(31) Poddubny, A.; Iorsh, I.; Belov, P.; Kivshar, Y., Hyperbolic metamaterials. *Nat. Photonics* **2013,** *7* (12), 948-957.
(32) Huang, J.; Li, L.; Lu, P.; Qi, Z.; Sun, X.; Zhang, X.; Wang, H., Self-assembled Co-BaZrO3 nanocomposite thin films with ultra-fine vertically aligned Co nanopillars. *Nanoscale* **2017,** *9* (23), 7970-7976.
(33) Huang, J.; Qi, Z.; Li, L.; Wang, H.; Xue, S.; Zhang, B.; Zhang, X.; Wang, H., Self-assembled vertically aligned Ni nanopillars in CeO2 with anisotropic magnetic and transport properties for energy applications. *Nanoscale* **2018,** *10* (36), 17182-17188.
(34) Zhang, B.; Huang, J.; Jian, J.; Rutherford, B. X.; Li, L.; Misra, S.; Sun, X.; Wang, H., Tuning magnetic anisotropy in Co–BaZrO3 vertically aligned nanocomposites for memory device integration. *Nanoscale Advances* **2019,** *1* (11), 4450-4458.
(35) Kalaswad, M.; Zhang, B.; Wang, X.; Wang, H.; Gao, X.; Wang, H., Integration of highly anisotropic multiferroic BaTiO3–Fe nanocomposite thin films on Si towards device applications. *Nanoscale Advances* **2020**.
(36) Ramesh, R.; Spaldin, N. A., Multiferroics: progress and prospects in thin films. *Nature Materials* **2007,** *6* (1), 21-29.
(37) Spaldin, N. A.; Ramesh, R., Advances in magnetoelectric multiferroics. *Nature Materials* **2019,** *18* (3), 203-212.
(38) Grollier, J.; Querlioz, D.; Stiles, M. D., Spintronic Nanodevices for Bioinspired Computing. *Proc. IEEE* **2016,** *104* (10), 2024-2039.
(39) Armelles, G.; Cebollada, A.; García-Martín, A.; González, M. U., Magnetoplasmonics: Combining Magnetic and Plasmonic Functionalities. *Advanced Optical Materials* **2013,** *1* (1), 10-35.
(40) Wang, X.; Jian, J.; Diaz-Amaya, S.; Kumah, C. E.; Lu, P.; Huang, J.; Lim, D. G.; Pol, V. G.; Youngblood, J. P.; Boltasseva, A.; Stanciu, L. A.; O'Carroll, D. M.; Zhang, X.; Wang, H., Hybrid plasmonic Au–TiN vertically aligned nanocomposites: a nanoscale platform towards tunable optical sensing. *Nanoscale Advances* **2019,** *1* (3), 1045-1054.
(41) Wang, X.; Jian, J.; Zhou, Z.; Fan, C.; Dai, Y.; Li, L.; Huang, J.; Sun, J.; Donohue, A.; Bermel, P.; Zhang, X.; Chen, H. T.; Wang, H., Self-Assembled Ag–TiN Hybrid Plasmonic Metamaterial: Tailorable Tilted Nanopillar and Optical Properties. *Advanced Optical Materials* **2018,** *7* (3), 1801180.
(42) Huang, J.; Wang, X.; Hogan, N. L.; Wu, S.; Lu, P.; Fan, Z.; Dai, Y.; Zeng, B.; Starko-Bowes, R.; Jian, J.; Wang, H.; Li, L.; Prasankumar, R. P.; Yarotski, D.; Sheldon, M.; Chen, H. T.; Jacob, Z.; Zhang, X.; Wang, H., Nanoscale Artificial Plasmonic Lattice in Self-Assembled Vertically Aligned Nitride-Metal Hybrid Metamaterials. *Adv. Sci.* **2018,** *5* (7), 1800416.
(43) Wang, H.; Zhang, X.; Gupta, A.; Tiwari, A.; Narayan, J., Growth and characteristics of TaN/TiN superlattice structures. **2003,** *83* (15), 3072.
(44) Wang, X. J.; Nguyen, T.; Cao, Y.; Jian, J.; Malis, O.; Wang, H. Y., AlN-based hybrid thin films with self-assembled plasmonic Au and Ag nanoinclusions. *Appl. Phys. Lett.* **2019,** *114* (2), 5.

(45) Milosev, I.; Strehblow, H. H.; Navinsek, B., Comparison of TiN, ZrN and CrN hard nitride coatings: Electrochemical and thermal oxidation. *Thin Solid Films* **1997,** *303* (1-2), 246-254.
(46) Veprek, S.; Reiprich, S., A concept for the design of novel superhard coatings. *Thin Solid Films* **1995,** *268* (1-2), 64-71.
(47) Wang, H.; Tiwari, A.; Kvit, A.; Zhang, X.; Narayan, J., Epitaxial growth of TaN thin films on Si(100) and Si(111) using a TiN buffer layer. **2002,** *80* (13), 2323.
(48) Khatkhatay, F.; Jian, J.; Jiao, L.; Su, Q.; Gan, J.; Cole, J. I.; Wang, H., Diffusion barrier properties of nitride-based coatings on fuel cladding. *Journal of Alloys and Compounds* **2013,** *580*, 442-448.
(49) Garcia, A. S.; Diniz, J. A.; Swart, J. W.; Lima, L. P. B.; Puydinger Dos Santos, M. V. In *Formation and characterization of tin layers for metal gate electrodes of CMOS capacitors*, 2014; IEEE.
(50) Naik, G. V.; Shalaev, V. M.; Boltasseva, A., Alternative Plasmonic Materials: Beyond Gold and Silver. *Advanced Materials* **2013,** *25* (24), 3264-3294.
(51) Naik, G. V.; Schroeder, J. L.; Ni, X.; Kildishev, A. V.; Sands, T. D.; Boltasseva, A., Titanium nitride as a plasmonic material for visible and near-infrared wavelengths. *Opt. Mater. Express* **2012,** *2* (4), 478-489.
(52) Boltasseva, A.; Atwater, H. A., Low-Loss Plasmonic Metamaterials. *Science* **2011,** *331* (6015), 290-291.
(53) Zilio, P.; Malerba, M.; Toma, A.; Zaccaria, R. P.; Jacassi, A.; Angelis, F. D., Hybridization in Three Dimensions: A Novel Route toward Plasmonic Metamolecules. *Nano Lett.* **2015,** *15* (8), 5200-5207.
(54) Yu, Q.; Guan, P.; Qin, D.; Golden, G.; Wallace, P. M., Inverted Size-Dependence of Surface-Enhanced Raman Scattering on Gold Nanohole and Nanodisk Arrays. *Nano Lett.* **2008,** *8* (7), 1923-1928.
(55) Luo, J.; Zeng, B.; Wang, C.; Gao, P.; Liu, K.; Pu, M.; Jin, J.; Zhao, Z.; Li, X.; Yu, H.; Luo, X., Fabrication of anisotropically arrayed nano-slots metasurfaces using reflective plasmonic lithography. *Nanoscale* **2015,** *7* (44), 18805-18812.
(56) Shkondin, E.; Repan, T.; Takayama, O.; Lavrinenko, A. V., High aspect ratio titanium nitride trench structures as plasmonic biosensor. *Opt. Mater. Express* **2017,** *7* (11), 4171-4182.
(57) Li, W.; Guler, U.; Kinsey, N.; Naik, G. V.; Boltasseva, A.; Guan, J. G.; Shalaev, V. M.; Kildishev, A. V., Refractory Plasmonics with Titanium Nitride: Broadband Metamaterial Absorber. *Advanced Materials* **2014,** *26* (47), 7959-+.
(58) Gui, L. L.; Bagheri, S.; Strohfeldt, N.; Hentschel, M.; Zgrabik, C. M.; Metzger, B.; Linnenbank, H.; Hu, E. L.; Giessen, H., Nonlinear Refractory Plasmonics with Titanium Nitride Nanoantennas. *Nano Lett.* **2016,** *16* (9), 5708-5713.
(59) Liu, H.; Liu, T.; Zhang, L.; Han, L.; Gao, C.; Yin, Y., Etching-Free Epitaxial Growth of Gold on Silver Nanostructures for High Chemical Stability and Plasmonic Activity. *Advanced Functional Materials* **2015,** *25* (34), 5435-5443.
(60) Hao, Q.; Li, W.; Xu, H.; Wang, J.; Yin, Y.; Wang, H.; Ma, L.; Ma, F.; Jiang, X.; Schmidt, O. G.; Chu, P. K., VO2 /TiN Plasmonic Thermochromic Smart Coatings for Room-Temperature Applications. *Advanced Materials* **2018,** *30* (10), 1705421.
(61) Vispute, R. D.; Wu, H.; Narayan, J., High quality epitaxial aluminum nitride layers on sapphire by pulsed laser deposition. *Appl. Phys. Lett.* **1995,** *67* (11), 1549-1551.

(62) Yang, H.; Wang, W.; Liu, Z.; Li, G., Epitaxial growth of 2 inch diameter homogeneous AlN single-crystalline films by pulsed laser deposition. *Journal of Physics D: Applied Physics* **2013,** *46* (10), 105101.
(63) Vitos, L.; Ruban, A. V.; Skriver, H. L.; Kollar, J., The surface energy of metals. *Surf. Sci.* **1998,** *411* (1-2), 186-202.
(64) Wang, X.; Ma, X.; Shi, E.; Lu, P.; Dou, L.; Zhang, X.; Wang, H., Large-Scale Plasmonic Hybrid Framework with Built-In Nanohole Array as Multifunctional Optical Sensing Platforms. *Small* **2020**, e1906459.
(65) Anker, J. N.; Hall, W. P.; Lyandres, O.; Shah, N. C.; Zhao, J.; Van Duyne, R. P., Biosensing with plasmonic nanosensors. *Nature Materials* **2008,** *7* (6), 442-453.
(66) Yu, C.; Irudayaraj, J., Multiplex Biosensor Using Gold Nanorods. *Analytical Chemistry* **2007,** *79* (2), 572-579.
(67) Li, X.-M.; Bi, M.-H.; Cui, L.; Zhou, Y.-Z.; Du, X.-W.; Qiao, S.-Z.; Yang, J., 3D Aluminum Hybrid Plasmonic Nanostructures with Large Areas of Dense Hot Spots and Long-Term Stability. *Advanced Functional Materials* **2017,** *27* (10), 1605703.
(68) Hultman, L.; Bareño, J.; Flink, A.; Söderberg, H.; Larsson, K.; Petrova, V.; Odén, M.; Greene, J. E.; Petrov, I., Interface structure in superhard TiN-SiN nanolaminates and nanocomposites: Film growth experiments and ab initio calculations. **2007,** *75* (15).
(69) Chen, A.; Bi, Z.; Tsai, C.-F.; Chen, L.; Su, Q.; Zhang, X.; Wang, H., Tilted Aligned Epitaxial La0.7Sr0.3MnO3 Nanocolumnar Films with Enhanced Low-Field Magnetoresistance by Pulsed Laser Oblique-Angle Deposition. *Crystal Growth & Design* **2011,** *11* (12), 5405-5409.
(70) Kesapragada, S. V.; Victor, P.; Nalamasu, O.; Gall, D., Nanospring Pressure Sensors Grown by Glancing Angle Deposition. *Nano Lett.* **2006,** *6* (4), 854-857.
(71) Liu, Y. J.; Chu, H. Y.; Zhao, Y. P., Silver Nanorod Array Substrates Fabricated by Oblique Angle Deposition: Morphological, Optical, and SERS Characterizations. *The Journal of Physical Chemistry C* **2010,** *114* (18), 8176-8183.
(72) Rycenga, M.; Cobley, C. M.; Zeng, J.; Li, W.; Moran, C. H.; Zhang, Q.; Qin, D.; Xia, Y., Controlling the synthesis and assembly of silver nanostructures for plasmonic applications. *Chemical reviews* **2011,** *111* (6), 3669-712.
(73) Haghtalab, M.; Tamagnone, M.; Zhu, A. Y.; Safavi-Naeini, S.; Capasso, F., Ultrahigh Angular Selectivity of Disorder-Engineered Metasurfaces. *ACS Photonics* **2020,** *7* (4), 991-1000.
(74) Coenen, T.; Vesseur, E. J. R.; Polman, A., Deep Subwavelength Spatial Characterization of Angular Emission from Single-Crystal Au Plasmonic Ridge Nanoantennas. *ACS Nano* **2012,** *6* (2), 1742-1750.
(75) Aimon, N. M.; Choi, H. K.; Sun, X. Y.; Kim, D. H.; Ross, C. A., Templated Self-Assembly of Functional Oxide Nanocomposites. *Advanced Materials* **2014,** *26* (19), 3063-3067.
(76) Fan, M.; Zhang, B.; Wang, H.; Jian, J.; Sun, X.; Huang, J.; Li, L.; Zhang, X.; Wang, H., Self-Organized Epitaxial Vertically Aligned Nanocomposites with Long-Range Ordering Enabled by Substrate Nanotemplating. *Advanced Materials* **2017,** *29* (23), 1606861.
(77) Bozhevolnyi, S. I.; Khurgin, J. B., The case for quantum plasmonics. *Nat. Photonics* **2017,** *11* (7), 398-400.
(78) Jacob, Z.; Shalaev, V. M., Plasmonics Goes Quantum. *Science* **2011,** *334* (6055), 463-464.
(79) Tame, M. S.; McEnery, K. R.; Özdemir, Ş. K.; Lee, J.; Maier, S. A.; Kim, M. S., Quantum plasmonics. *Nature Physics* **2013,** *9* (6), 329-340.

(80) Shahjamali, M. M.; Zhou, Y.; Zaraee, N.; Xue, C.; Wu, J.; Large, N.; McGuirk, C. M.; Boey, F.; Dravid, V.; Cui, Z.; Schatz, G. C.; Mirkin, C. A., Ag-Ag2S Hybrid Nanoprisms: Structural versus Plasmonic Evolution. *ACS Nano* **2016,** *10* (5), 5362-73.
(81) Losurdo, M.; Bergmair, I.; Dastmalchi, B.; Kim, T. H.; Giangregroio, M. M.; Jiao, W. Y.; Bianco, G. V.; Brown, A. S.; Hingerl, K.; Bruno, G., Graphene as an Electron Shuttle for Silver Deoxidation: Removing a Key Barrier to Plasmonics and Metamaterials for SERS in the Visible. *Advanced Functional Materials* **2014,** *24* (13), 1864-1878.
(82) Kauranen, M.; Zayats, A. V., Nonlinear plasmonics. *Nat. Photonics* **2012,** *6* (11), 737-748.
(83) Kinsey, N.; Syed, A. A.; Courtwright, D.; Devault, C.; Bonner, C. E.; Gavrilenko, V. I.; Shalaev, V. M.; Hagan, D. J.; Van Stryland, E. W.; Boltasseva, A., Effective third-order nonlinearities in metallic refractory titanium nitride thin films. **2015,** *5* (11), 2395.
(84) Kim, Y. S.; Song, J.; Hwang, C.; Wang, X.; Wang, H.; MacManus-Driscoll, J. L.; Song, H.-K.; Cho, S., Nanoporous Films and Nanostructure Arrays Created by Selective Dissolution of Water-Soluble Materials. *Advanced Science* **2018,** *5* (11), 1800851.
(85) Im, H.; Lee, S. H.; Wittenberg, N. J.; Johnson, T. W.; Lindquist, N. C.; Nagpal, P.; Norris, D. J.; Oh, S. H., Template-Stripped Smooth Ag Nanohole Arrays with Silica Shells for Surface Plasmon Resonance Biosensing. *Acs Nano* **2011,** *5* (8), 6244-6253.
(86) Masson, J. F.; Murray-Methot, M. P.; Live, L. S., Nanohole arrays in chemical analysis: manufacturing methods and applications. *Analyst* **2010,** *135* (7), 1483-1489.
(87) Jiang, P.; McFarland, M. J., Wafer-scale periodic nanohole arrays templated from two-dimensional nonclose-packed colloidal crystals. *J. Am. Chem. Soc.* **2005,** *127* (11), 3710-3711.
(88) Henzie, J.; Lee, M. H.; Odom, T. W., Multiscale patterning of plasmonic metamaterials. *Nature Nanotechnology* **2007,** *2* (9), 549-554.
(89) Ebbesen, T. W.; Lezec, H. J.; Ghaemi, H. F.; Thio, T.; Wolff, P. A., Extraordinary optical transmission through sub-wavelength hole arrays. *Nature* **1998,** *391* (6668), 667-669.
(90) De Leebeeck, A.; Kumar, L. K. S.; de Lange, V.; Sinton, D.; Gordon, R.; Brolo, A. G., On-chip surface-based detection with nanohole arrays. *Analytical Chemistry* **2007,** *79* (11), 4094-4100.
(91) Im, H.; Lesuffleur, A.; Lindquist, N. C.; Oh, S. H., Plasmonic Nanoholes in a Multichannel Microarray Format for Parallel Kinetic Assays and Differential Sensing. *Analytical Chemistry* **2009,** *81* (8), 2854-2859.
(92) Escobedo, C., On-chip nanohole array based sensing: a review. *Lab Chip* **2013,** *13* (13), 2445-2463.
(93) Martin-Moreno, L.; Garcia-Vidal, F. J.; Lezec, H. J.; Pellerin, K. M.; Thio, T.; Pendry, J. B.; Ebbesen, T. W., Theory of extraordinary optical transmission through subwavelength hole arrays. *Phys. Rev. Lett.* **2001,** *86* (6), 1114-1117.
(94) Ding, F.; Pors, A.; Bozhevolnyi, S. I., Gradient metasurfaces: a review of fundamentals and applications. *Rep. Prog. Phys.* **2018,** *81* (2), 44.
(95) Meinzer, N.; Barnes, W. L.; Hooper, I. R., Plasmonic meta-atoms and metasurfaces. *Nat. Photonics* **2014,** *8* (12), 889-898.
(96) González-Díaz, J. B.; García-Martín, A.; Armelles, G.; Navas, D.; Vázquez, M.; Nielsch, K.; Wehrspohn, R. B.; Gösele, U., Enhanced Magneto-Optics and Size Effects in Ferromagnetic Nanowire Arrays. *Advanced Materials* **2007,** *19* (18), 2643-2647.
(97) Khurgin, J. B., How to deal with the loss in plasmonics and metamaterials. *Nature Nanotechnology* **2015,** *10* (1), 2-6.

(98) Khurgin, J. B.; Boltasseva, A., Reflecting upon the losses in plasmonics and metamaterials. *MRS bulletin* **2012,** *37* (8), 768-779.
(99) Jahani, S.; Jacob, Z., All-dielectric metamaterials. *Nature Nanotechnology* **2016,** *11* (1), 23-36.
(100) West, P. R.; Ishii, S.; Naik, G. V.; Emani, N. K.; Shalaev, V. M.; Boltasseva, A., Searching for better plasmonic materials. *Laser Photon. Rev.* **2010,** *4* (6), 795-808.
(101) Naik, G. V.; Kim, J.; Boltasseva, A., Oxides and nitrides as alternative plasmonic materials in the optical range [Invited]. *Opt. Mater. Express* **2011,** *1* (6), 1090.
(102) X. Wang, H. H. W., J. Jian, B. X. Rutherford, X. Gao, X. Xu, X. Zhang, H. Wang, Metal-free oxide-nitride heterostructure as a tunable hyperbolic metamaterial platform. *Nanoletters* **2020**.

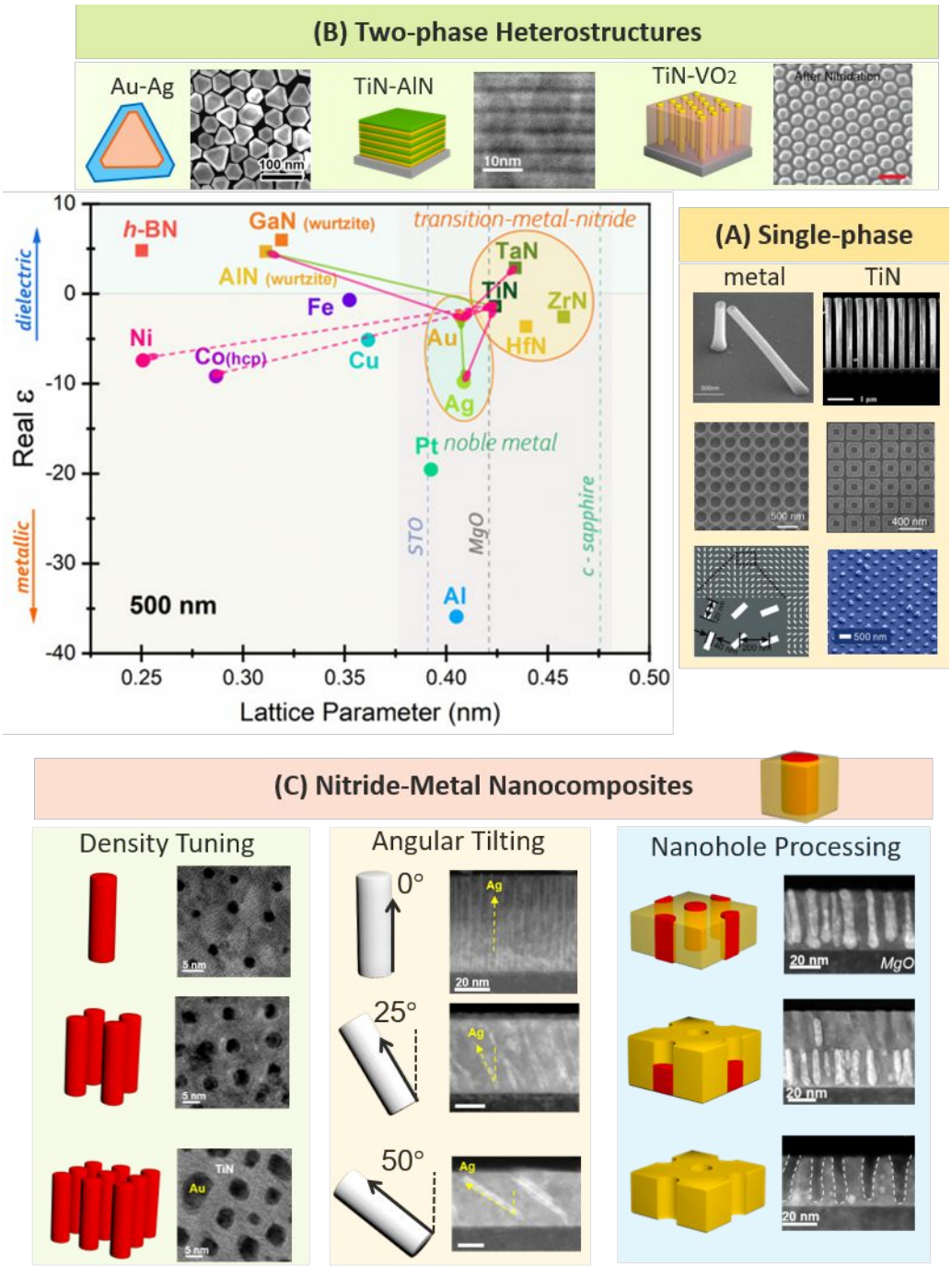

Figure 1. Lattice parameter versus ε_1 plot of metals and nitrides. (A) Past achievements in metal and TiN nanoplasmonics.[53-58] Reproduced with permissions, ref. 55, Royal Society of Chemistry, copyright 2015, ref. 57, John Wiley and Sons, copyright 2014. (B) Examples on two-phase hybrid plasmonics.[43, 59-60] Reproduced with permissions, ref 59, John Wiley and Sons, copyright 2015, ref 60, John Wiley and Sons, copyright 2018. (C) Schematic illustration on nitride-metal nanocomposites, tailorable and designable geometries.[40-41, 64] Reproduced with permissions, ref. 41, John Wiley and Sons, copyright 2018, ref. 64, John Wiley and Sons, copyright 2020.

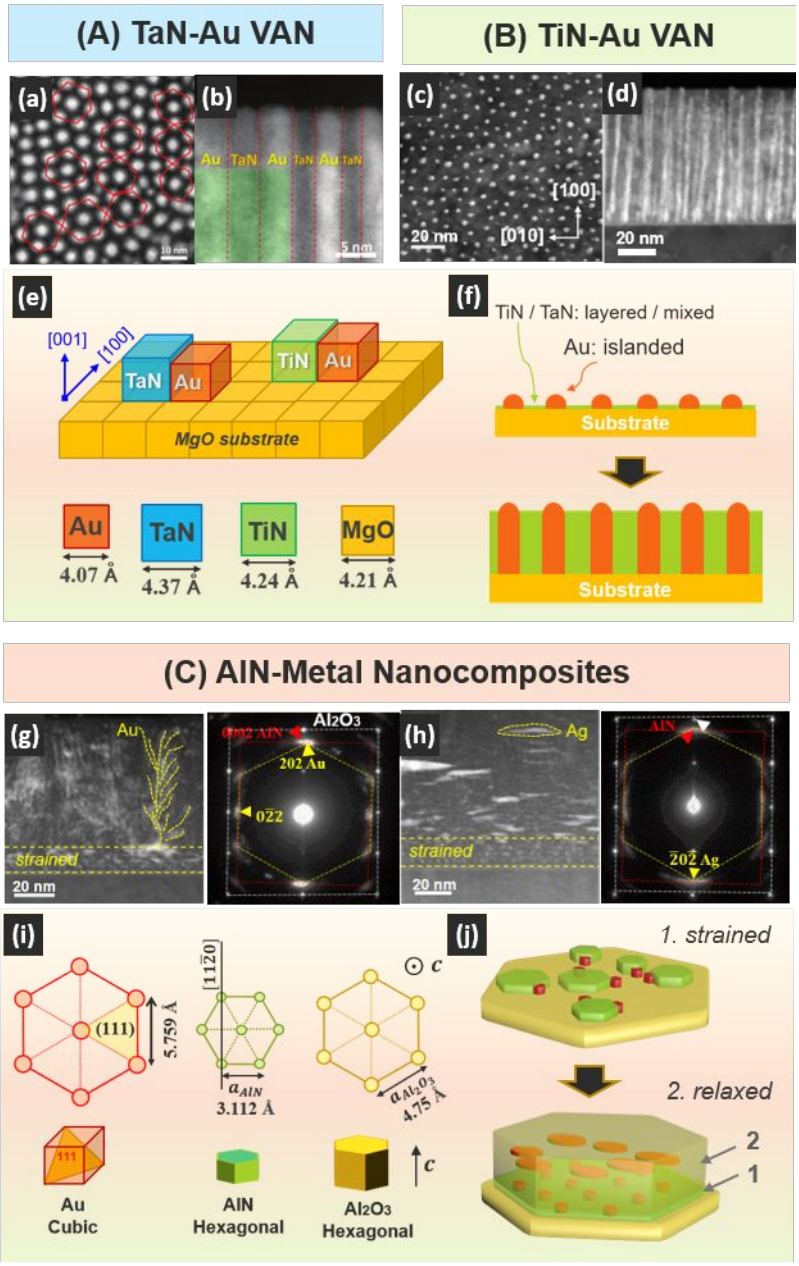

Figure 2. (A,B) TaN-Au and TiN-Au VANs.[40, 42] (a,b) STEM micrographs of TaN-Au VAN. (c,d) STEM micrographs TiN-Au VAN. (e) Lattice parameters and crystal symmetries of Au, TiN, TaN and MgO. (f) 2D illustration of TiN/TaN-metal VAN growth. (C) Wurtzite AlN-metal nanocomposites. (g) AlN-Au STEM micrograph and corresponding SAED patterns from <1$\bar{1}$ 00>.[44] Reproduced with permission, AIP Publishing, copyright 2019. (h) AlN-Ag STEM micrograph and corresponding SAED patterns from <1$\bar{1}$00>. (i) Crystal symmetry and lattice parameter of Au, AlN and Al_2O_3. (j) 3D illustration on two-step growth of AlN-metal nanocomposites.

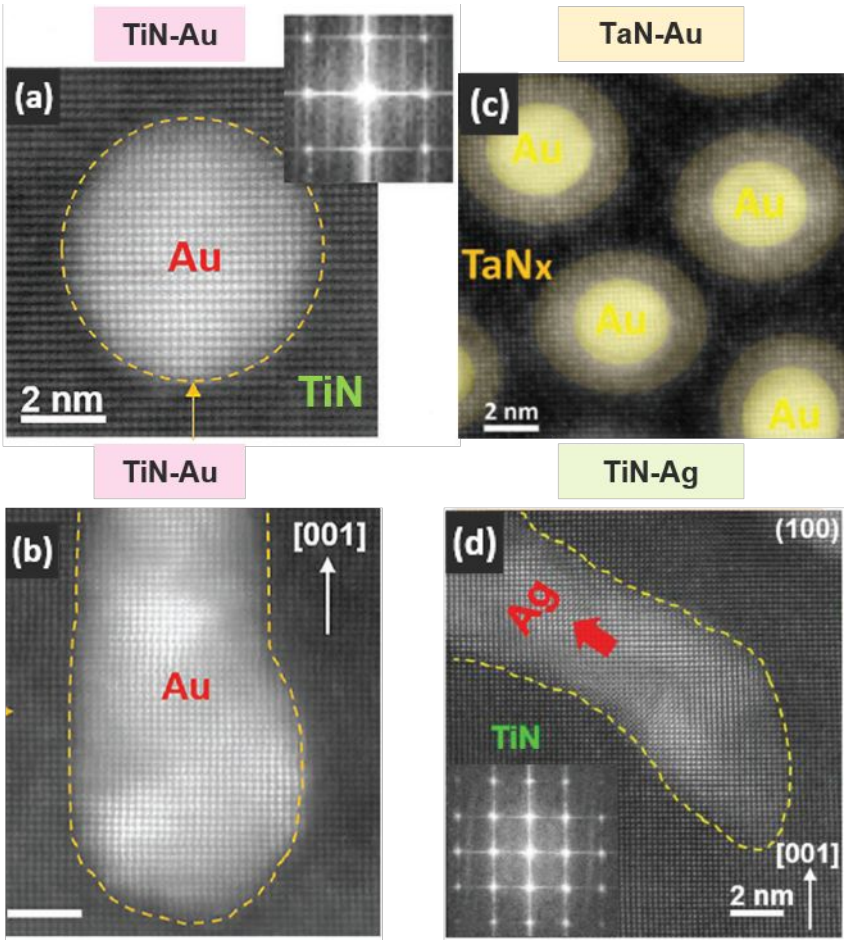

Figure 3. HRSTEM micrographs at nitride/metal interfaces. (a,b) Plan view and cross-sectional images of TiN-Au VAN.[64] (c) Plan view image of TaN-Au VAN.[42] (d) Cross-sectional image of tilted TiN-Ag nanocomposite.[41] Reproduced with permission, ref. 41, John Wiley and Sons, copyright 2018.

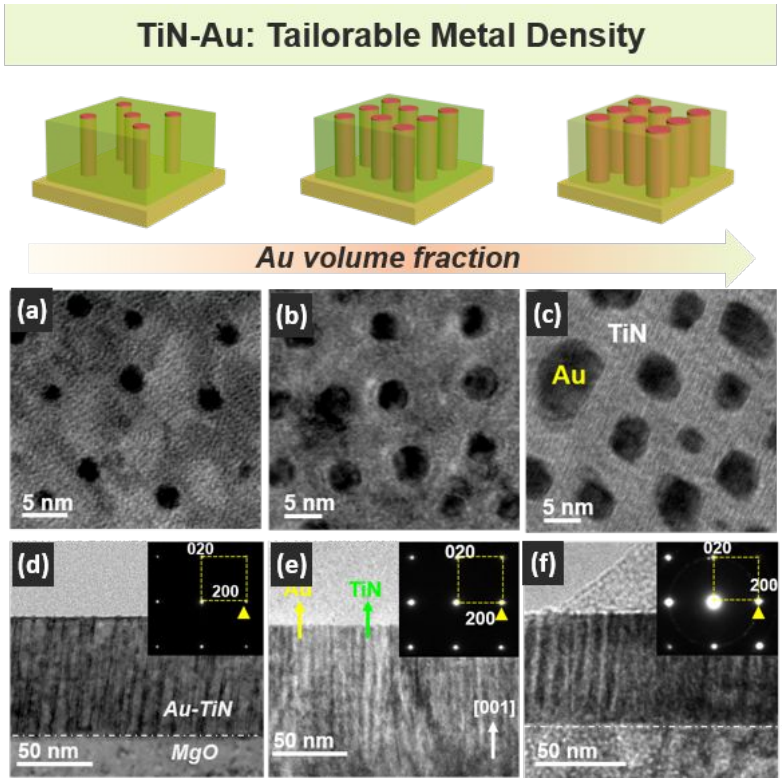

Figure 4. TiN-Au VANs with tailored Au density. (a-c) Plan view and (d-f) cross-sectional TEM micrographs of three TiN-Au VANs with gradual change of Au volume fraction.[40]

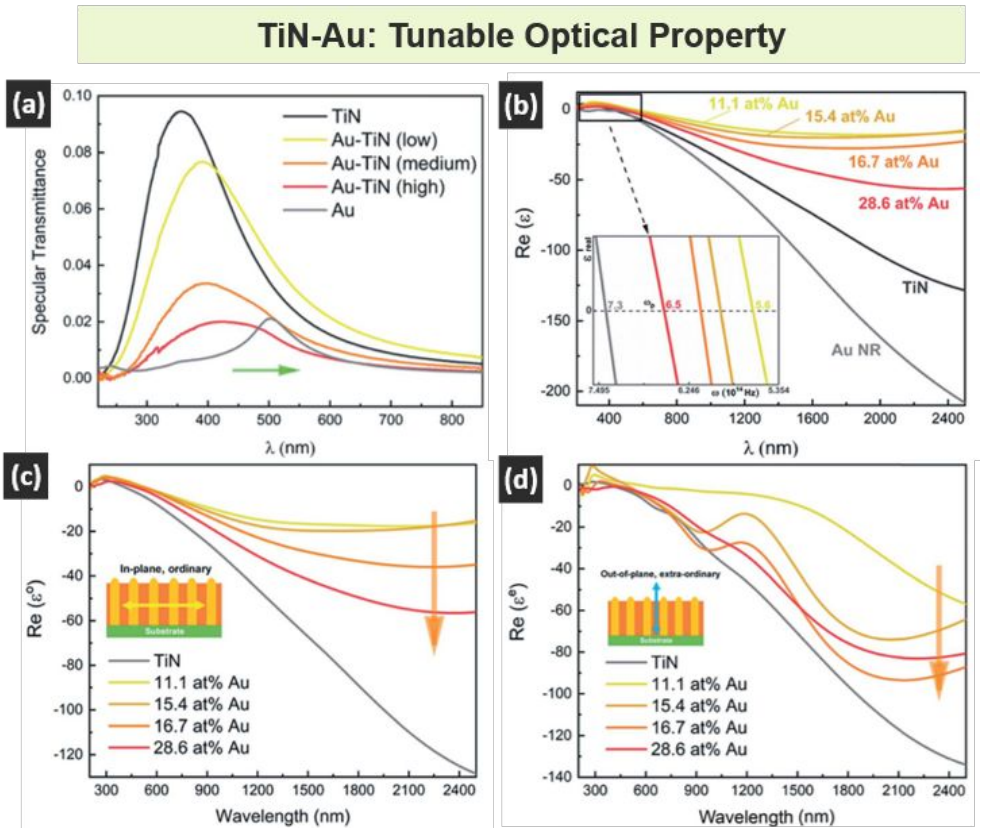

Figure 5. TiN-Au with tunable optical properties. (a) Transmittance spectra of TiN-Au VANs as well as pure TiN and Au films. (b) Real-part dielectric function of five samples, inset shows the zoomed image of plasmon frequency. (c,d) Ordinary and extraordinary real-part dielectric function retrieved from uniaxial model.[40]

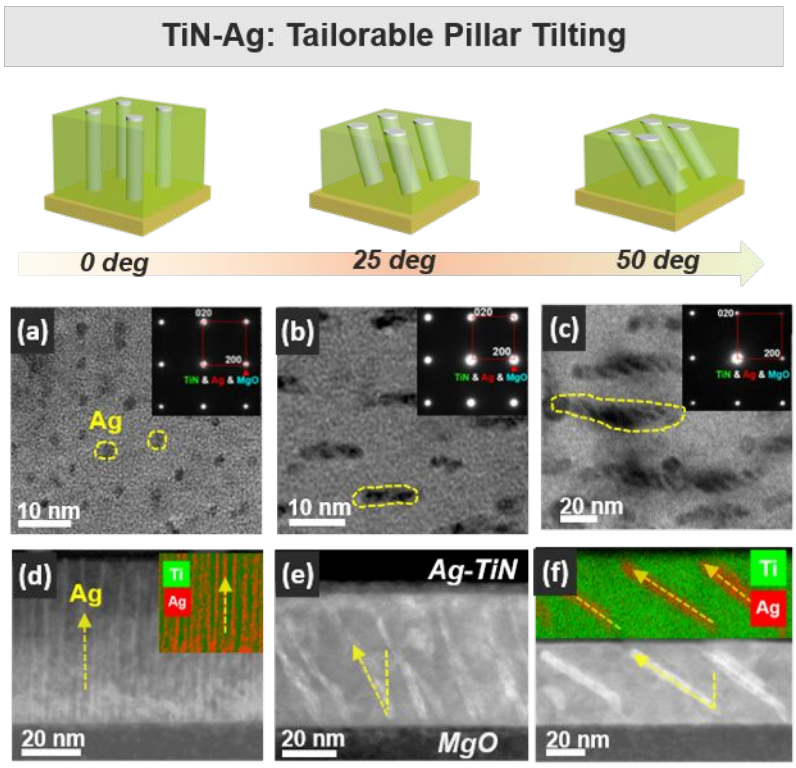

Figure 6. Microstructure of TiN-Ag nanocomposites with tailored tilting angles of Ag nanopillars. (a-c) Plan view TEM and (d-f) cross-sectional STEM micrographs, insets show the diffraction patterns and EDX mapping.[41] Reproduced with permission, John Wiley and Sons, copyright 2018.

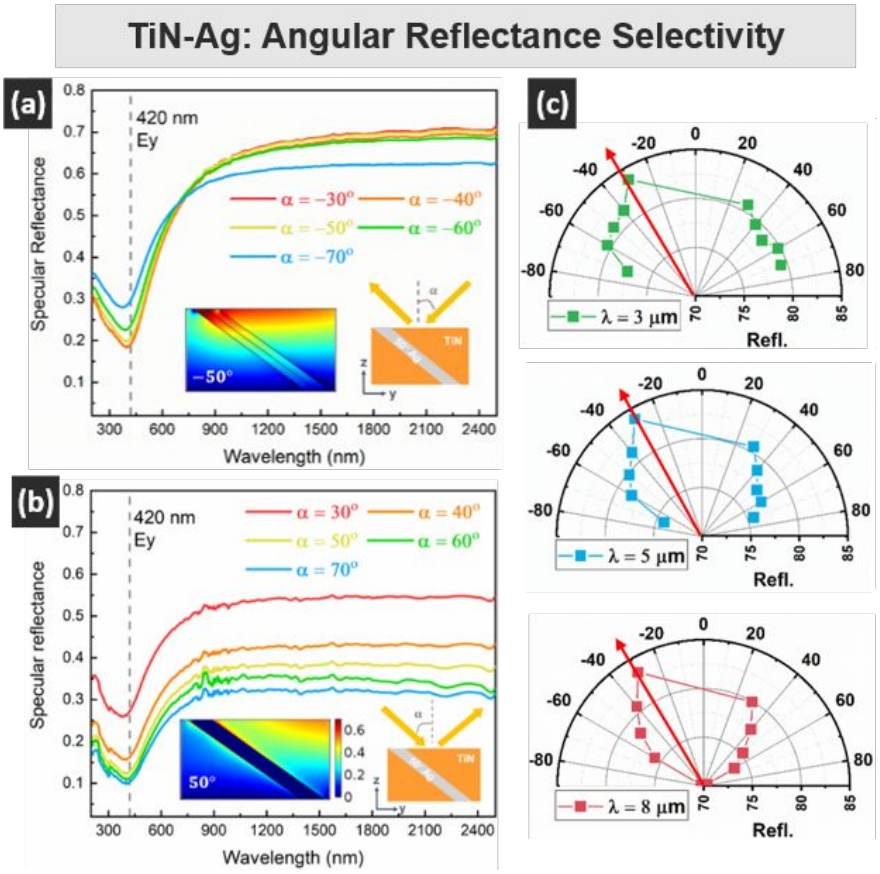

Figure 7. Angular reflectance selectivity of tilted TiN-Ag at UV-infrared regime. (a,b) Angular dependent optical reflectance spectra measured at two different sample alignment with 180° rotation. Insets show the electric field distribution and illustrations. (c) Polar plots at 3, 5, 8 μm showing angular dependence of reflectance intensity.[41] Reproduced with permission, John Wiley and Sons, copyright 2018.

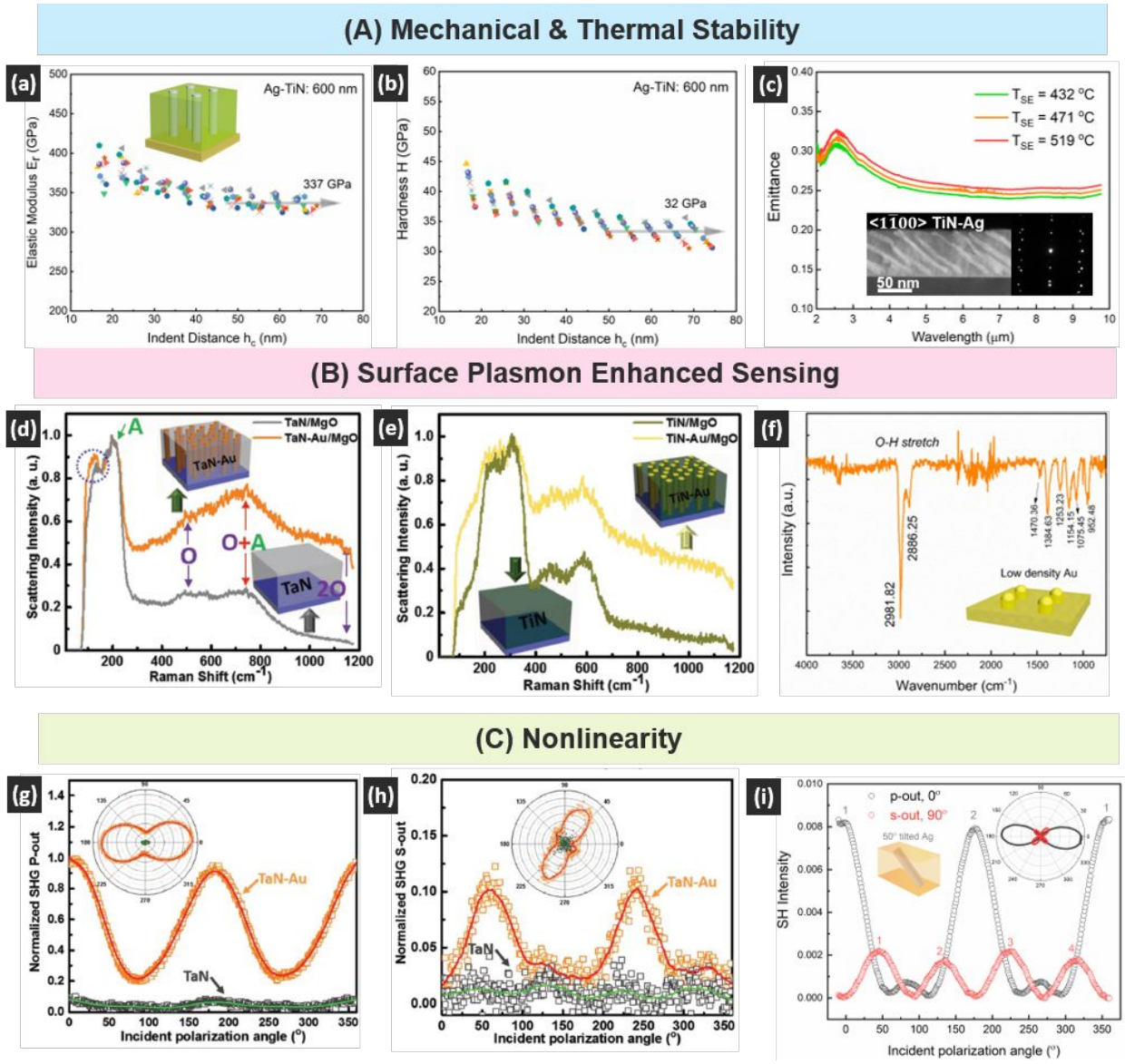

Figure 8. Multifunctionalities of nitride-metal nanocomposites, including (A) mechanical and thermal stability, (B) surface plasmon enhanced sensing, (C) nonlinearity. (a-c) Elastic modulus, hardness and high-temperature emittance spectra of TiN-Ag nanocomposite, inset of (c) shows the microstructure after thermal treatment.[41] (d-e) Raman spectra collected on TaN-Au and TiN-Au VANs.[42] (f) Fourier-transform infrared spectroscopy (FTIR) spectrum of chemical treated TiN-Au surface.[40] (g-h) SHG signals of p-output and s-output directions measured for TaN-Au VAN.[42] (i) p- and s-output SHG signal of TiN-Ag nanocomposite thin film.[41] Reproduced with permission, ref. 41, John Wiley and Sons, copyright 2018.

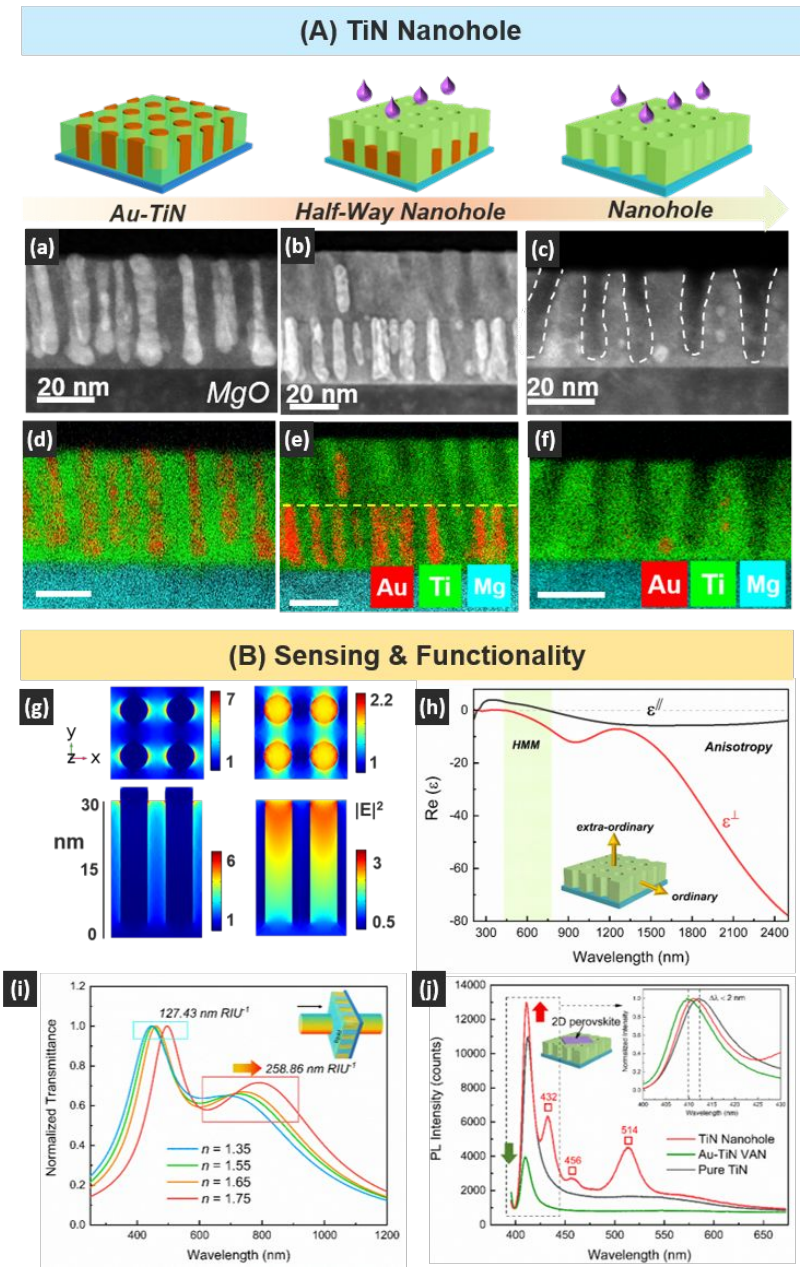

Figure 9. Large-scale plasmonic TiN nanoholes.[64] Reproduced with permission, John Wiley and sons, copyright 2020. (A) Microstructure. (a-f) Illustrations and real STEM and EDX images of TiN-Au (before etching), half-way etched nanohole, and the TiN nanohole (after etching). (B) Sensing and functionalities. (g) Electric field mapping before and after etching. (h) Dielectric function of TiN nanohole film. (i) Transmittance spectra with changing of refractive index. (j) Photoluminescence spectra of 2D perovskite nanoplates coupling with TiN nanoholes, pure TiN and TiN-Au thin film.

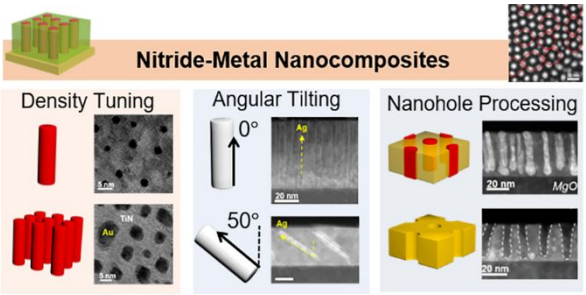

Self-assembled Nitride-metal nanocomposites offering flexible geometrical control and tunable functionalities towards metamaterial design and nanophotonic devices.